6.6 GRAVITY WAVE PROPAGATION THROUGH TIME-DEPENDENT SHEAR

JULIE C. VANDERHOFF *
Brigham Young University, Provo, Utah

ABSTRACT

Small-scale internal gravity waves can affect large scale atmospheric motions. A parameterization of their influence is necessary to understand the mesosphere and lower thermosphere thermal structure and constituent transport. Mixing induced by dissipating gravity waves in the atmosphere is important to the vertical transport of chemicals, energy, and momentum, which when transferred in large amounts to the local mean flow plays a central role in driving the mean meridional circulation. In addition, global circulation patterns in the middle atmosphere including the quasi-biennial oscillation of the equatorial lower stratosphere and the semiannual oscillations of the equatorial upper stratosphere and mesosphere are driven by the drag and diffusion caused by internal wave breaking. These internal waves can encounter many other phenomena, the most widely studied being a steady shear background wind. Although this is realistic, it is not the whole picture. Large-scale inertial frequency waves over a short time period act much like a steady shear, but are time-dependent and influence small-scale gravity wave propagation in a dynamically different way than a steady shear. The waves which may generally reach a critical level (where their relative frequency approaches zero) and distribute their momentum to the mean flow, do not because the critical level generated by the inertial wave is not steady. The effects of time-dependent shear are quantified through linear, Wentzel-Kramers-Brillouin (WKB) ray theory, with which thousands of waves are tested, and complemented by fully nonlinear numerical simulations of a few representative waves. It is found that internal gravity waves interacting with inertial waves are continually being shifted, altered, and break in different regions. These waves have the propensity to distribute their energy hundreds of kilometers from their expected location if that position is calculated only taking into account constant winds. The result is a significant shift in probable breaking locations of waves and changes in overall momentum flux of the waves throughout their propagation. Some waves gain energy, some lose energy, and some are unaffected, but shifted spatially. Others may even break during the interaction with the inertial wave, dissipating their energy prematurely. The investigation of momentum fluxes of smaller-scale internal waves within larger mesoscale inertial gravity waves is accomplished. Probable interactions are identified and results are quantified.

1. Introduction

Internal waves are continuously generated and breaking throughout the atmosphere. Strong generation regions include mountain ranges, convection, wind shear, adjustment of unbalanced flows near jet streams and frontal systems, and body forcing accompanying localized wave dissipation (Fritts and Alexander (2003)). Wave breaking can effectively mix pollutants through the atmosphere and may contribute to driving some larger-scale flows. Gravity waves are affected by other waves, winds, and the changing stratification as they propagate. Each of these interactions, in addition to gravity wave dissipation, may contribute to the vertical flux of horizontal momentum and the universal frequency spectrum, slopes near $-5/4$, seen in the middle atmosphere (VanZandt (1982); Balsley and Carter (1982); Nakamura, Tsuda, Fukao, Kato, Manson, and Meek (1993); Collins, Nomura, and Gardner (1994)). The importance of each of these individual interactions is unknown and the resulting spectral shapes and wave breaking are not well understood (Gardner (1996)).

Internal gravity waves with frequencies near the Coriolis frequency are inertial waves. These waves have long horizontal wavelengths (up to 3000km in the troposphere (Ratnam, Babu, Rao, Rao, and Rao (2008))) and much shorter vertical wavelengths ($1-$ 7km). These scales are larger in the troposphere and

*Corresponding author address: Julie C. Vanderhoff, Mechanical Engineering Department, Brigham Young University, 435 CTB, Provo, UT, 84602-4201. (email: jvanderhoff@byu.edu).

decrease in the lower stratosphere. These waves can be propagating either upward or downward. Zhang and Yi (2007) found the tropospheric jet generated an equal number of upward and downward traveling inertial waves. These waves are similar to a time dependent shear. Other internal gravity waves interacting with these inertial waves lead to unsteady critical levels (Sartelet (2003a,b)) or strong refraction (Broutman, Macaskill, McIntyre, and Rottman (1997); Vanderhoff, Nomura, Rottman, and Macaskill (2008); Sonmor and Klaasen (2000)) depending on the relative size and direction between the waves.

This study attempts to characterize interactions between high frequency internal gravity waves and inertial waves. Both fully non-linear numerical simulations and ray theory are utilized to understand a range of cases. We assume internal gravity waves of a range of scales are propagating upward through an inertial wave with energy propagating in either the same or opposite direction. The inertial wave propoerties are defined by Serafimovich, Zülicke, Hoffmann, Peters, Dalin, and Singer (2006) and Guest, Reeder, Marks, and Karoly (2000). Results quantify interactions between these waves and define which small-scale waves will continue to propagate upwards into the upper stratosphere, which will have a change in their properties as they continue upward, and which will break.

In the next section, background information on the idealized problem and solution methods, ray tracing, and numerical simulations, is presented. In Section 3 the results of small-scale wave propagation through different mediums is addressed for both ray tracing and numerical simulations. Conclusions are drawn in Section 4.

2. Setup

In this section we will cover the different setups of the ray tracing calculations and numerical simulations.

a. The idealized problem

In the ray tracing and numerical simulations we consider the case of a packet of high frequency waves approaching a single inertia packet either from above or below, as described in Vanderhoff, Nomura, Rottman, and Macaskill (2008), and shown in Fig.1. The coordinate system is (x, y, z) with z positive upwards, x positive eastward, and y positive northward. We assume that the buoyancy frequency N and the Coriolis parameter f are both constant.

The inertial packet has wavenumber $\mathbf{K} = (0, 0, M)$, where $M = 2\pi/\lambda_i$ and λ_i is the vertical wavelength of the wave. The corresponding velocity field is uniform, horizontally, $\mathbf{u} = (u, v, 0)$, but confined in the vertical by a Gaussian envelope:

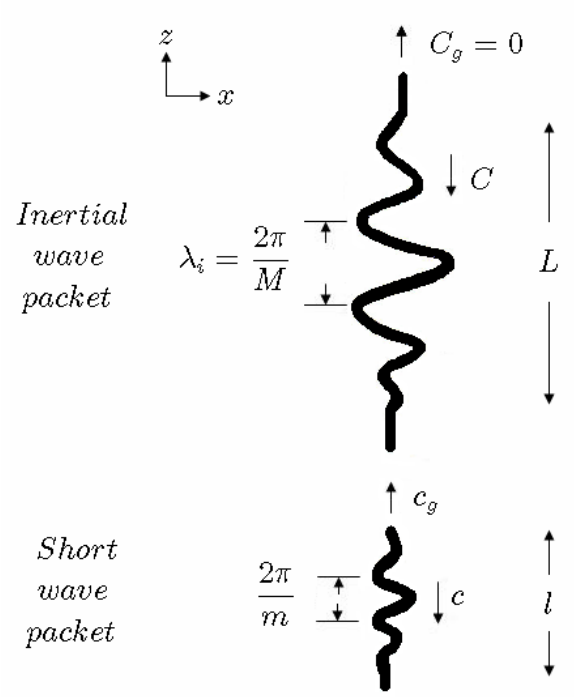

FIG. 1. Schematic of a short wave packet approaching an inertia-wave packet with basic parameters shown. (Capital letters denote inertial wave properties)

$$U + iV = U_0\, e^{-z^2/L^2} e^{i(Mz - ft)} \tag{1}$$

where L and U_0 are constants, real and complex respectively. The envelope of the inertia-wave packet assumed stationary, since the vertical component of the group velocity vanishes at the inertial frequency. The phases move vertically (either upward or downward) through the packet at speed $C = f/M$.

The high frequency waves have wavenumber $\mathbf{k} = (k, 0, m)$, with k constant, and intrinsic frequency $\hat{\omega}$, which is the Doppler-shifted frequency, where

$$\hat{\omega}^2 = (N^2k^2 + f^2m^2)/(k^2 + m^2) \tag{2}$$

We take m and $\hat{\omega}$ to be positive, and allow k to have either sign. The vertical group velocity $c_g = \partial\hat{\omega}/\partial m$ is negative if m is positive and positive if m is negative.

The vertical displacement of the high frequency waves is $\zeta = \zeta_0 \exp(i\theta)$, from which the wavenumber and wave frequency are given by $\mathbf{k} = \nabla\theta$ and $\omega = -\theta_t$, respectively, and where $\omega = \hat{\omega} + kU$. The wave-energy density E is related to ζ_0 by

$$E = \frac{1}{2}\rho_0 \zeta_0^2 N^2 \left[1 + \left(\frac{fm}{Nk}\right)^2\right] \qquad (3)$$

where ρ_0 is the mean density of the fluid.

The numerical simulations are initialized at time $t = 0$ with a short wave packet whose vertical displacement field $\zeta(x, z, t)$ has the initial form

$$\zeta(x, z, 0) = \mathrm{Re}\left\{\zeta_0\, e^{-(z-z_0)^2/\ell^2} e^{i(kx+mz)}\right\} \qquad (4)$$

where ℓ and z_0 are real constants and ζ_0 is a complex constant. The initial vertical position z_0 is specified such that the high frequency wave packet is below the inertia-wave packet since $c_g > 0$.

Wave-breaking is defined when isopycnals are vertical, $\zeta_z > 1$, leading to overturning within the fluid and resulting turbulence. This can be calculated in the numerical simulations by finding $\Delta\zeta/\Delta z$. For calculating wave steepness in ray theory we use the dispersion relation and (3) to derive:

$$\zeta_z = -m \left| \left(\frac{2A\hat{\omega}}{\rho_0}\right)^{1/2} N^{-1} \right| . \qquad (5)$$

Here $A = E/\hat{\omega}$ is the wave-action density.

For the ray tracing and numerical simulation results shown in this paper, we use the following range of atmospheric parameters: $M = 2\pi/(7000\,\mathrm{m})$, $k = 2\pi/(100000\,\mathrm{m})$ to $2\pi/(10000\,\mathrm{m})$, $f = 1.361 \times 10^{-4}\mathrm{s}^{-1}$ ($69.3\,\mathrm{deg}$ North), $N = 0.02\mathrm{s}^{-1}$, and $U_0 = 5$m/s for the inertial wave. For the numerical simulations, the initial steepness $|\zeta_z| = |m\zeta_0| = 0.1$, where subscript z represents the partial derivative with respect to z. We will alter the vertical wavenumber, m, to realize different group speeds of the short wave. The vertical wavelength never exceeds 30km so the change in background density over a wavelength is not significant in the calculations.

b. Ray Theory

Using ray theory we can calculate approximately the behavior of the high frequency wave encounter with the inertial wave group. To do this we assume that the inertial wave is unaffected by the short wave interaction. Another necessary assumption is that the inertial wave has a much larger length scale than that of the short wave, which is not always the case for these atmospheric waves. Thus the interaction is tested with the numerical simulations and since the result of these show the inertial waves is unchanged by the interaction with the higher frequency wave, ray tracing is used. Also we assume the short wave is determined by the linear dispersion relation. Then an evolution equation in characteristic form can be found for $\mathbf{k}$. For further detail see Vanderhoff et al. (2008).

1) THE RAY EQUATIONS

The ray-tracing results in this paper are obtained with the following pair of ray equations, for the vertical position of the ray path and the vertical wavenumber respectively:

$$\frac{d\mathbf{x}}{dt} = c_g + \mathbf{U}, \qquad \frac{dm}{dt} = -k\frac{\partial u}{\partial z} . \qquad (6)$$

Here $d/dt = \partial/\partial t + c_g \bullet \nabla$. Because the expression (1) has no dependence on x or y, the horizontal components $(k, 0)$ of the wavenumber of the short waves are conserved along the ray. These equations are solved using the Matlab ODE45 solver which is based on an explicit Runge-Kutta formula, the Dormand-Prince pair, Dormand and Prince (1980), which is a one-step solver. The tolerances are set at 10^{-4} for the relative error and 10^{-6} for the absolute error.

2) ANALYTIC RAY SOLUTIONS

An analytic ray solution describing high frequency wave refraction by inertia waves propagating opposite to the small scale waves appears in Broutman and Young (1986) and is obtained by letting L approach infinity in equation (1). The inertia-wave velocity $\mathbf{U}$ is then purely sinusoidal. In a reference frame moving at the inertial-wave phase speed C, the inertial current appears steady. Solutions then exist for which the high frequency wave has a frequency in the inertial-wave reference frame

$$\Omega = \hat{\omega} + kU - Cm \approx constant. \qquad (7)$$

When the vertical group speed of the high frequency wave is in the same direction as the inertial wave the result is transient critical levels. A critical level occurs when the relative frequency of the internal wave tends to the Coriolis frequency, f. Yet in this case no such levels exist When an inertial wave is present

$$\Omega = f + kU - Cm . \qquad (8)$$

When high frequency waves are traveling upward through the inertial wave the value of the horizontal phase speed at the critical level is merely a different sign if the wave is traveling in the positive or negative x-direction. If k is positive (high frequency wave traveling in positive x-direction, here traveling to the east) and m is negative (high frequency wave traveling upward), the value of the background velocity at the critical level is positive, and for upward, west traveling

waves, the background velocity at the critical level is also to the west.

When the high frequency waves are propagating opposite the the inertial wave caustic interactions occur. For our idealized model, caustics occur when

$$c_g = C \ . \tag{9}$$

Vanderhoff et al. (2008) show results for these types of interactions. Strong refraction may occur and enhanced amplitudes are expected at refraction sites. The most interesting final result occurs if the high frequency wave is initially traveling more slowly vertically than the inertial wave. In this case the high frequency extracts energy from the inertial wave and refracts to a higher frequency.

c. Numerical Simulations

Numerical results are obtained by integrating the fully nonlinear inviscid, Boussinesq equations of motion. In their vorticity-streamfunction form, these are:

$$\frac{\partial^2\psi}{\partial x^2} + \frac{\partial^2\psi}{\partial z^2} = q \tag{10}$$

$$\frac{\partial q}{\partial t} - J(\psi, q) - \frac{\partial \sigma}{\partial x} - f\frac{\partial v}{\partial z} = 0 \tag{11}$$

$$\frac{\partial v}{\partial t} - J(\psi, v) + fu = 0 \tag{12}$$

$$\frac{\partial \sigma}{\partial t} - J(\psi, \sigma) - N^2 w = 0, \tag{13}$$

where q is the y-component of vorticity and $J(\psi, q)$ the Jacobian with respect to (x, z). Here the fluid velocity $\mathbf{u} = (u, v, w)$, and the stream function ψ is defined such that $u = \partial\psi/\partial z$, $w = -\partial\psi/\partial x$, and $q = \partial u/\partial z - \partial w/\partial x$. The scaled density perturbation due to the presence of internal wave motions is $\sigma = g\rho'/\rho_0$ where g is the acceleration due to gravity; the density $\rho = \rho' + \rho_0$, with $\rho_0(z)$ the mean density profile. Because of rotation, there is a nonzero v field, but all variables are assumed to be independent of y. The scale height is not included because the relatively small vertical scale of the waves results in insignificant changes in density over the height of the wave.

Periodic boundary conditions are imposed in both the x- and z-directions, and the equations are solved using a Fourier spectral collocation technique with Runge-Kutta time stepping. The computational domain contains one horizontal wavelength of the high frequency waves in the horizontal direction and one vertical wavelength of the inertia waves in the vertical direction.

There are 512 grid points in the vertical direction, but only 16 grid points in the horizontal direction. The low horizontal resolution suffices for this problem – as has been verified by tests at higher resolution – because the high frequency waves, though strongly refracted, are not strongly amplified, and remain well below breaking threshold. The maximum wave-steepness $\partial\zeta/\partial z$ of the high frequency waves over the duration of the simulation does not exceed unity (except in a special case as discussed later). No viscosity or filtering was necessary to stabilize the calculations.

3. Results

Results of the numerical simulations are presented first to provide justification for use of ray theory for the statistical calculations.

a. Numerical simulations through an inertial wave

Figure 2 shows the fully nonlinear numerical simulation of a high frequency wave propagating through an inertial wave going in the same direction. The group speed of the inertial wave cannot be seen in the simulations due to the very slow speed. The high frequency wave vertical wavelength is 5000 m and the horizontal wavelength is 100000 m. The inertial wave vertical wavelength is 7000 m and the horizontal wavelength is 1000000 m. The inertial wave is in the center of the domain. As the high frequency wave interacts both waves seem slightly affected, but after the short wave has propagated through, the inertial wave is unchanged. The high frequency wave has spread slightly, as can be seen in both plots in Fig. 2, though only slightly for this case. Since waves are traveling in the same direction an unsteady critical level is approached from afar, but not reached. Here, with an inertial wave maximum horizontal velocity of 5 m/s and the value for a critical level at approximately $16m/s$, even an unsteady critical level approach will not be strong. This can be seen by the lack of an increase in the perturbation density of the waves. If an unsteady critical level were approached, where the background horizontal velocity was greater than the necessary condition, a significant increase in perturbation density of the high frequency wave would be expected. In this case, it is not expected due to the low horizontal velocity of the inertial wave. Since observed inertial waves have low horizontal velocities, critical levels may not be approached.

Figure 3 is the wave steepness of the interaction from Fig. 2. It can be seen the steepness within the interaction increases, but does not increase over unity (which defines wave breaking). Thus an assumption of no wave breaking can be made. This is also necessary to successfully utilize two-dimesional and linear

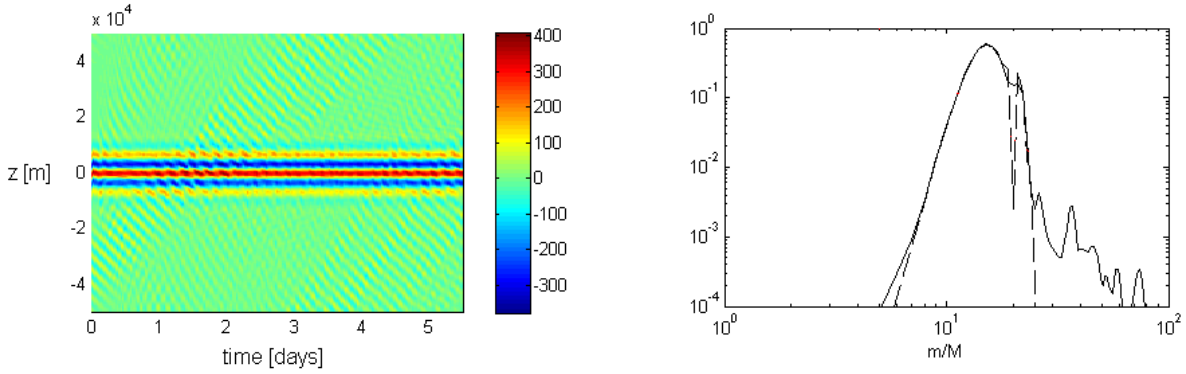

FIG. 2. Fully nonlinear numerical simulation of a high frequency wave propagating through an inertial wave. Both waves are propagating in the same direction. Left is the perturbation density. Right is the vertical wavenumber spectra. Initial spectra are shown with dashed line, and final is solid line.

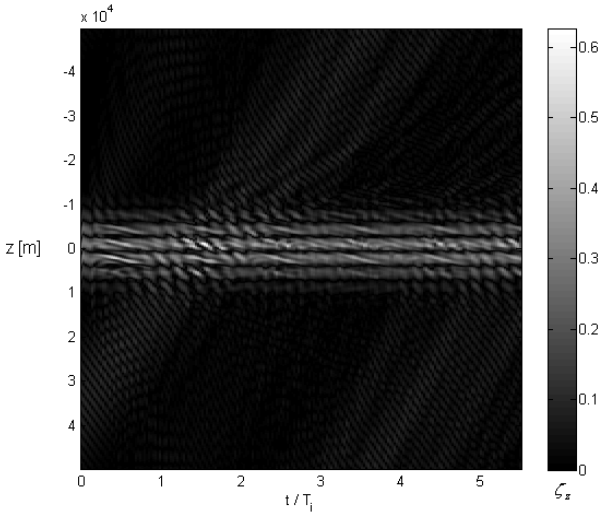

FIG. 3. Wave steepness for simulations of Fig. 2.

theory as breaking is both three-dimensional and nonlinear. The specifics of this interaction must be studied in further detail for a better understanding of the dynamics during the interaction. Since the final output results in an unchanged inertial wave and a high frequency wave that has slightly spread (as expected) it assumed ray theory can be used for conclusions about parts of this type of interaction.

When the inertial wave is propagating downward the high frequency wave spreads more, but the inertial wave again stays unchanged. This can be seen in Fig. 4. This increased spreading is expected and was found by Vanderhoff et al. (2008) when the inertial wave was modeled as an unsteady background shear with no density perturbation associated. The high frequency wave refracts strongly while inside the inertial wave and can leave with new properties. Here the waves have generally spread to higher frequencies. This is most likely due to the dynamics of the refraction. At a higher frequency the waves propagate faster in the vertical and are more likely to escape the inertial wave envelope. Thus the basic dynamics of the interaction are captured while the inertial wave sustains no changes. Again the steepness increases during the interaction (not shown), but not to a level where breaking is expected. These simulations of waves propagating in opposite directions where only the high frequency waves are permanantly affected support the use of ray tracing for further study of these interactions.

The vertical flux of horizontal momentum is captured in the numerical simulations through calculating $u'w'$. Figure 5a shows $u'w'$ averaged over the first half of the time domain for the interaction when the waves are propagating in the same direction. Averaging over the first half of the interaction effectively captures the single interaction before the wave enters again due to the periodic boundary conditions. It can be seen that the average of the oscillations from the wave motion average to just over zero before the interaction, and slightly higher afterwards. Thus there has been an increase in the vertical flux of horizontal momentum for the interaction. Figure 5b shows the case where the waves are propagating in the opposite direction. Here the average vertical flux of horizontal momentum is negative initially, due to some initial transients from the generation of the large scale wave (currently trying to be resolved). After the interaction, though, the average has definitely increased as expected due to strong refraction.

Numerical simulations have shown what will be expected from other wave interactions which will be studied using ray theory. Waves propagating in the same direction may increase in amplitude slightly during the interaction, but are expected to be basically unmodified due to the interactions. Waves propagating in opposite directions may result in high frequency waves increasing in amplitude during the interaction, but after the interaction it should decrease due to the spreading of the wave spatially and among different frequencies. Wave spreading is dependent upon initial properties and location of the high frequency waves.

b. Ray Tracing through an inertial wave

When the inertial wave is defined with a vertical wavelength of 7000 m (Guest et al. (2000)) and maximum horizontal velocity of 5 m/s, results of ray tracing two high frequency waves are shown in Fig. 6. The high frequency waves are defined by $m = 2\pi/5000$ and $k = 2\pi/100000$. Figure 6a shows the path of the waves. Both are initially propoagating upward, but the solid line is a wave interacting with an inertial wave which is also propagating upward, whereas the dashed line represents an interaction with a downward propagating inertial wave. The region of action is much smaller than the envelope of the inertial wave due to the slow horizontal velocity of the inertial wave. The high frequency waves are unaffected except near the maximum velocity of the inertial wave. Both types of interactions show the high frequency waves affected by the inertial wave, but when both waves are propagating in the same direction there are only small changes in the high frequency wave propagation. It looks as if it just waves as it begins to approach a critical level, but then the critical level disappears. The waves propagating in opposite directions result in strong refraction, as seen in Vanderhoff et al. (2008). Figure 6c displays the change in the vertical wavenumber throughout the interaction. It can be seen that in the case where waves are propagating in the same direction there is no net change in the vertical wavenumber. Yet in the case where the waves are propagating in opposite vertical directions there is a final increase in the vertical wavelength which corresponds to an increase in vertical group velocity of the high frequency waves and thus an increase in the vertical flux of horizontal momentum.

As the rays are strongly refracted, resulting in the turning seen in Fig. 6a, the wave action density (amplitude squared) increases as seen in Fig. 6b. Although the amplitude is undefined with the current equations, the maximum amplitude is calculated using an Airy function patching technique described in Vanderhoff et al. (2008). Here the maximum wave action density normalized by its initial value is found to be 3.46, which corresponds to wave steepness only about three and a half times the initial, Fig. 6d. None of these

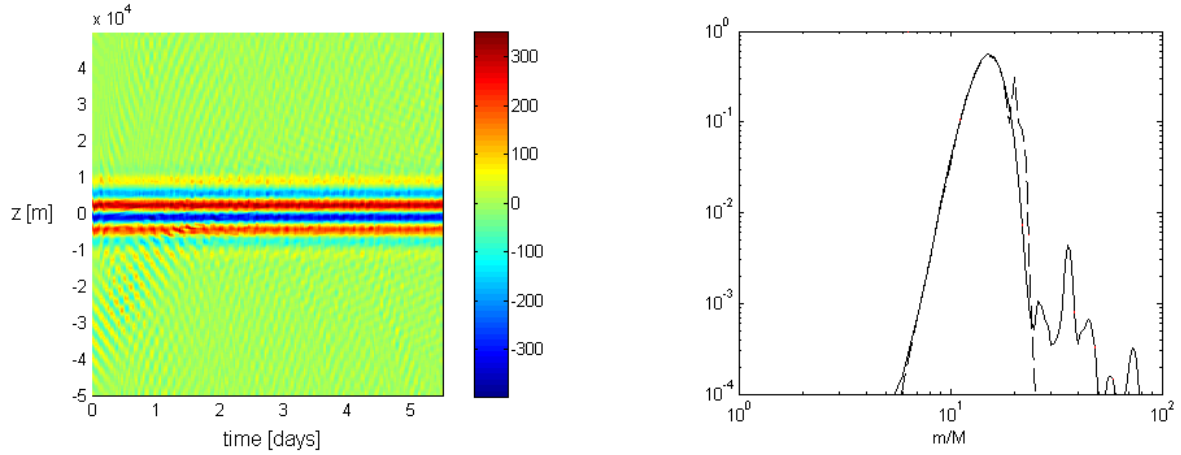

FIG. 4. As in Fig. 2 but where the high frequency and inertial wave are propagating in opposite directions.

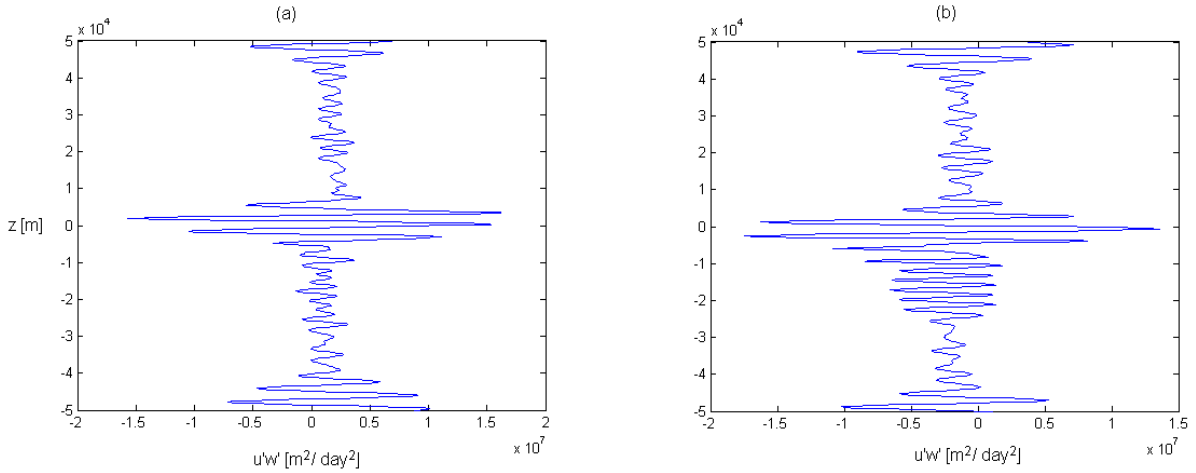

FIG. 5. Vertical flux of horizontal momentum ($\overline{u'w'}$) averaged over the first half of the time domain. (a) represents the case where the waves are propagating in the same direction, as in Fig. 2. (b) represents the case where the waves are propagating in opposite directions, as in Fig. 4.

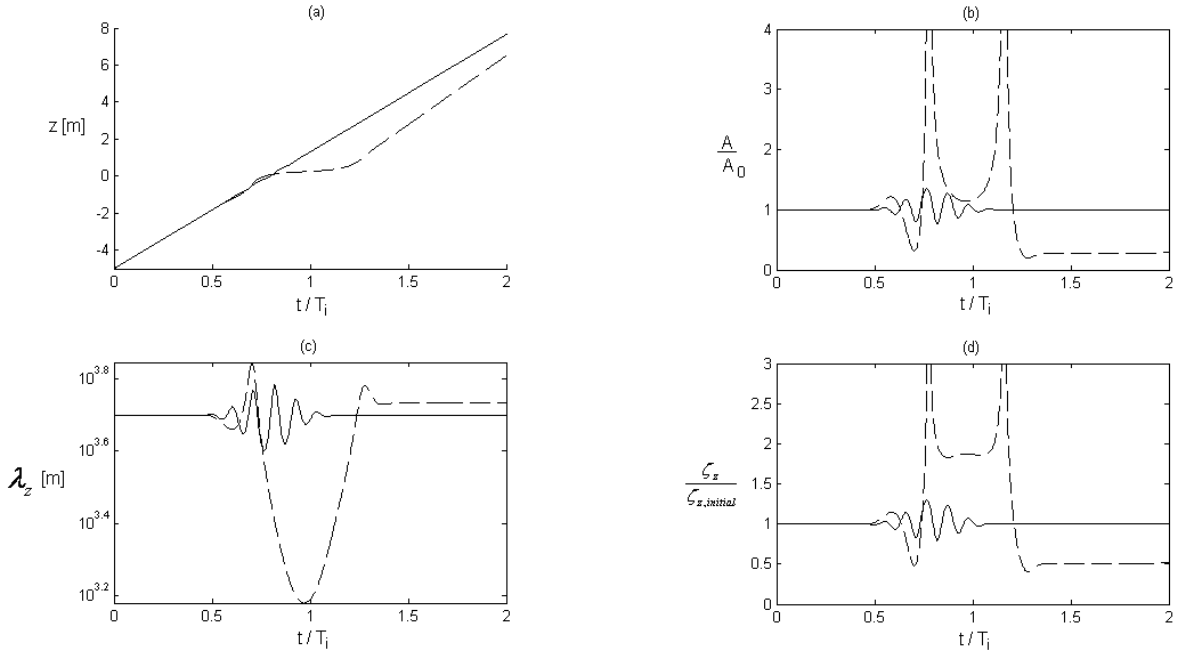

FIG. 6. High frequency waves propagating through an inertial wave with vertical wavelength of 7000 m and frequency $1.72 \times 10^{-4} s^{-1}$. Solid lines for both waves propagating in the same direction. Dashed lines represent waves propagating in opposite directions. (a) is the location of the waves as they propagate. (b) shows the wave action density normalized by the initial value. (c) is the changing vertical wavelength of the high frequency wave. (d) is the wave steepness normalized by the initial value.

waves seem likely to break due to the interaction (as was postulated previously from the numerical simulations).

As in Fritts and Alexander (2003), the vertical flux of horizontal momentum, $\bar{u'w'} = c_{gz}E/\hat{\omega}$ which can be easily applied to ray tracing. Averaging only over the interaction, the second wave in Fig. 7 actually has an decrease in vertical flux of horizontal momentum. This is due to the strong refraction to slow vertical group velocity during the interaction, and corresponds to the drop in vertical wavelength seen in Fig. 6c. Yet just after the interaction the vertical flux of horizontal momentum has increased by about 20%.

For the case when the inertial wave has a smaller vertical wavelength than the high frequency wave as in Serafimovich, Zülicke, Hoffmann, Peters, Dalin, and Singer (2006), Fig. 8 and Fig. 9 show the corresponding rays and their changing properties. It can be seen that here the first location of refraction does not appear as strong as in the previous case. This is due to the inertial wave envelope. The high frequency wave is approaching a caustic, but due to the still opening envelope the velocity necessary quickly propagates through and the refraction site is not as strong as expected. Thus the amplitude does not increase to infinity and a true caustic is not reached. But the second interaction is a strong refraction site. Here the amplitude increases, but again we can calculate the maximum amplitude which it is near 3. This wave, too, is not likely to break due to the refraction occurring during the interaction, but does result in an increase in vertical flux of horizontal momentum for the high frequency wave. Here the increase is near 30%.

Thus far the general ray tracing results have compared well with the numerical simulations. Thus we take the next step and utilize the advantage to ray theory: the ability to test thousands of cases in a matter of minutes.

Figure 10a and 10b are the total change in vertical flux of horizontal momentum for $10,000$ rays when the inertial wave has a vertical wavelength of 4600 m and 7000 m respectively. On the average initially slowly traveling vertical waves exit the interaction with an increased overall vertical flux of horizontal momentum. The specific increase is dependent on the initial position of the internal wave and actual initial vertical group velocity. The slowest waves can increase over ten times the original and the faster waves can decrease over ten times. The data cross the line of unchanging flux where the vertical group velocity of the high frequency waves is equal to the vertical phase speed, C, of the inertial wave. Waves which significantly change in energy flux are those interacting with a downward propagating inertial wave. These waves strongly refract and can result in a permanant change in wave properties. High frequency waves with vertical group velocities up to 25 m/s were tested, but waves with an initial group velocity over 2 m/s did not have a significant change in momentum flux over the interaction.

4. Discussion

In an attempt to better understand how unsteady shear affects high frequency waves in the atmosphere ray tracing and fully nonlinear numerical simulations were accomplished. Ray tracing results related well to fully nonlinear numerical simulations of situations expected in the atmosphere. This set a basis for the use of ray theory for further estimations of internal wave behavior. High frequency waves were set to interact with an inertial wave either propagating upward or downward. When upward propagating high frequency waves interacted with an upward propagating inertial wave the high frequency wave was spread slightly to both higher and lower frequencies. The general result, however, was an unchanged high frequency wave which was unlikely to break during the interaction. When waves were propagating in opposite directions, the high frequency waves studied in detail here had a net increase in the vertical flux of horizontal momentum due to the interaction. Although during the interaction it decreased. Due to the weak velocities of the inertial waves in the atmosphere, high frequency wave steepness during the interaction did not reach critical levels and the waves are expected to continue propagating past the inertial wave.

High frequency waves near the same vertical scale as inertial waves propagating upward in the atmosphere are pushed back and forth along with the background velocity, but for representative scales, no critical level is reached. It seems no critical level is even approached with such low horizontal velocities. When The representative waves studied here are propagating in opposite directions it is expected that the inertial wave effectively changes the vertical group speed of the lowest frequency waves. The very lowest increase in vertical flux of horizontal momentum, whereas those with initially faster group velocities (greater than the vertical phase speed of the inertial wave) may have a decrease. Yet many of the fastest high frequency waves, vertical group velocities above approximately 2 m/s, remained unaffected by inertial waves traveling in either direction.

REFERENCES

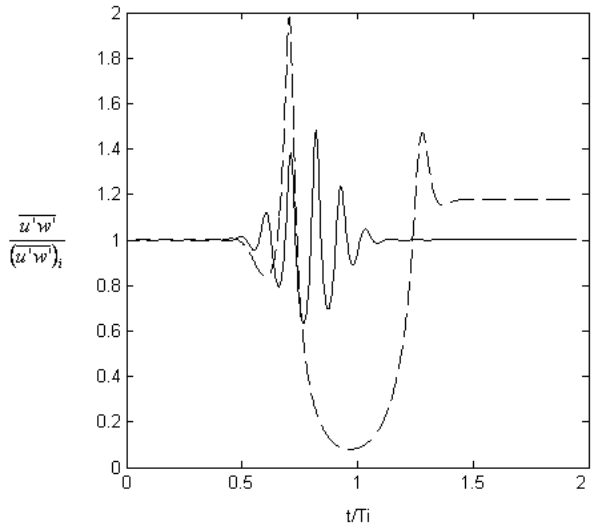

FIG. 7. Vertical flux of horizontal momentum for high frequency waves from Fig. 6 where solid and dashed lines have the same meaning.

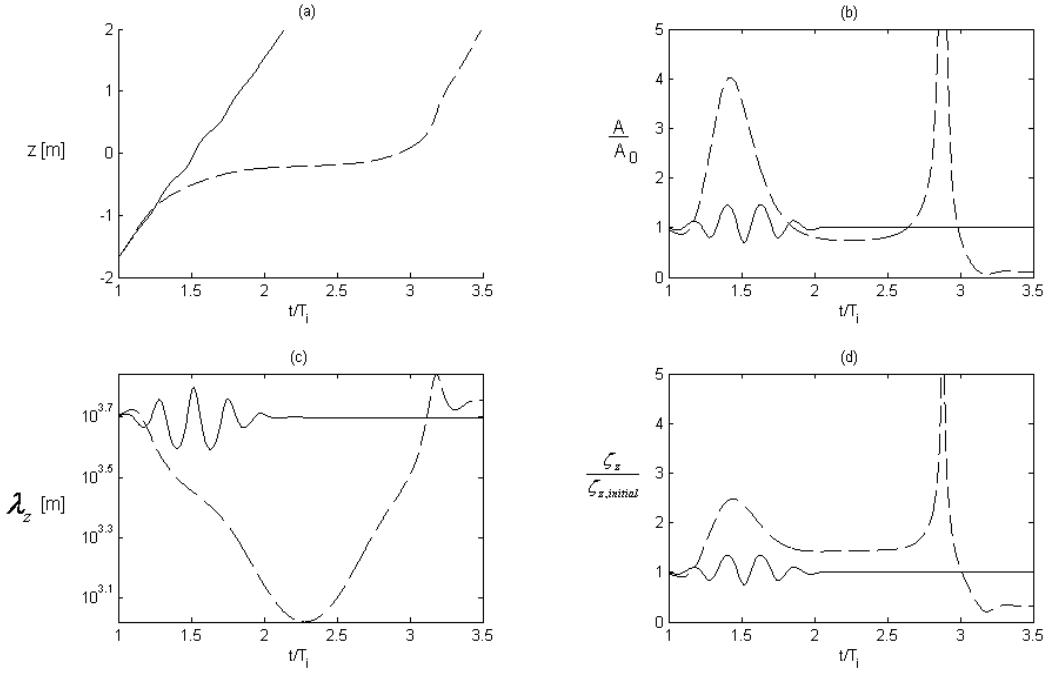

FIG. 8. Plots are as in Fig. 6. Inertial wave vertical wavelength is 4600 m.

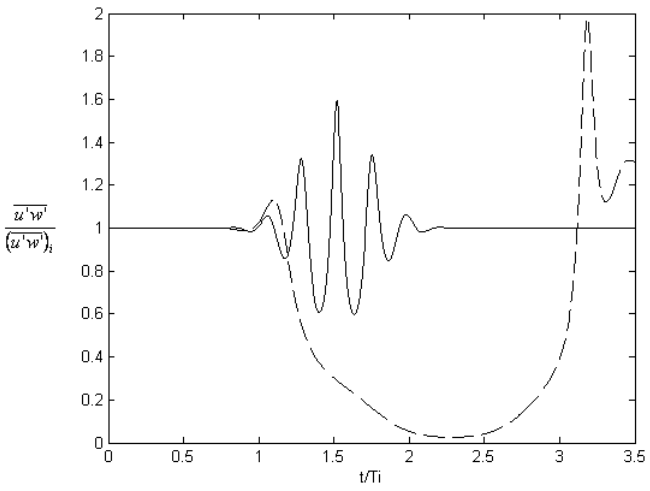

FIG. 9. Plots are as in Fig. 7. Inertial wave vertical wavelength is 4600 m and frequency is $3.12 \times 10^{-4} s^{-1}$.

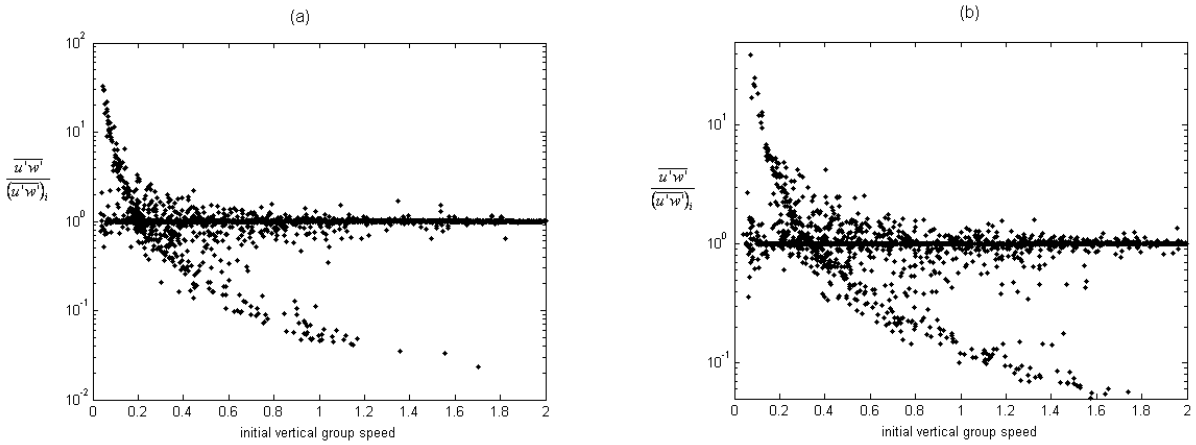

FIG. 10. Vertical flux of horizontal momentum after interaction normalized by initial in terms of high frequency wave initial vertical group speed. $10,000$ rays were traced through either an upward or downward propagating inertial wave and were started at random locations below the inertial wave packet. (a) Represents waves propagating through an inertial wave with vertical wavelength 4600 m and frequency $3.12 \times 10^{-4} s^{-1}$. (b) Represents waves propagating through an inertial wave with vertical wavelength 7000 m and frequency $1.72 \times 10^{-4} s^{-1}$.

Balsley, B. B., and Carter, D. A., 1982: The spectrum of atmospheric velocity fluctuations at 8 and 86 km. *Geophys. Res. Lett.*, **9**, 465–468.

Broutman, D., Macaskill, C., McIntyre, M. E., and Rottman, J. W., 1997: On doppler-spreading models of internal waves. *Geophys. Res. Lett.*, **24**, 2813–2816.

Broutman, D., and Young, W. R., 1986: On the interaction of small-scale oceanic internal waves with near-inertial waves. *J. Fluid Mech.*, **166**, 341–358.

Collins, R. L., Nomura, A., and Gardner, C. S., 1994: Gravity waves in the upper mesosphere over Antarctica: Lidar observations at the South Pole and Syowa. *J. Geophys. Res.*, **99**, 5475–5485.

Dormand, J. R., and Prince, P. J., 1980: A family of embedded Runge-Kutta formulae. *J. Comp. Appl. Math.*, **6**, 19–26.

Fritts, D. C., and Alexander, M. J., 2003: Gravity wave dynamics and effects in the middle atmosphere. *Rev. Geophys.*, **41**, 1003.

Gardner, C. S., 1996: Testing theories of atmospheric gravity wave saturation and dissipation. *J. Atmos. Terr. Phys.*, **58**, 1575–1589, doi:10.1016/0021-9169(96)00027-X.

Guest, F. M., Reeder, M. J., Marks, C. J., and Karoly, D. J., 2000: Inertia-gravity waves observed in the lower stratosphere over Macquarie Island. *J. Atmos. Sci.*, **57**, 737–752.

Nakamura, T., Tsuda, T., Fukao, S., Kato, S., Manson, A. H., and Meek, C. E., 1993: Comparative observations of short-period gravity waves (10-100 min) in the mesosphere in 1989 by Saskatoon MF radar (52^on), Canada and the MU radar (35^on), Japan. *Radio Sci.*, **28**, 729–746.

Ratnam, M. V., Babu, A. N., Rao, V. V. M. J., Rao, S. V. B., and Rao, D. N., 2008: MST radar and radiosonde observations of inertia-gravity wave climatology over tropical stations: Source mechanisms. *J. Geophys. Res.*, **113**, D07109, doi:10.1029/2007JD008986.

Sartelet, K. N., 2003a: Wave propagation inside an inertia wave. Part I: Role of time dependence and scale separation. *J. Atmos. Sci.*, **60**, 1433–1447.

Sartelet, K. N., 2003b: Wave propagation inside an inertia wave. Part II: Wave breaking. *J. Atmos. Sci.*, **60**, 1448–1455.

Serafimovich, A., Zülicke, C., Hoffmann, P., Peters, D., Dalin, P., and Singer, W., 2006: Inertia gravity waves in the upper troposphere during the MaCWAVE winter campaign - Pare II: Radar investigations and modelling studies. *Ann. Geophysicae*, **24**, 2863–2875.

Sonmor, L. J., and Klaasen, G., 2000: Mechanisms of gravity wave focusing in the middle atmosphere. *J. Atmos. Sci.*, **57**, 493–510.

Vanderhoff, J. C., Nomura, K. K., Rottman, J. W., and Macaskill, C., 2008: Doppler spreading of internal gravity waves by an inertia-wave packet. *J. Geophys. Res.*, **113**, C05018, doi:10.1029/2007JC004390.

VanZandt, T. E., 1982: A universal spectrum of buoyancy waves in the atmosphere. *Geophys. Res. Lett.*, **9**, 575–578.

Zhang, S. D., and Yi, F., 2007: Latitudinal and seasonal variations of inertial gravity wave activity in the lower atmosphere over central China. *J. Geophys. Res.*, **112**, D05109, doi:10.1029/2006JD007487.